Hall Drag and Magnetodrag in Graphene

Justin C. W. Song[1,2] and Leonid S. Levitov[1]

[1]*Department of Physics, Massachusetts Institute of Technology, Cambridge, Massachusetts 02139, USA*
[2]*School of Engineering and Applied Sciences, Harvard University, Cambridge, Massachusetts 02138, USA*

Massless Dirac fermions in graphene at charge neutrality form a strongly interacting system in which both charged and neutral (energy) modes play an important role. These modes are essentially decoupled in the absence of a magnetic field, but become strongly coupled when the field is applied. We show that this regime is characterized by strong magnetodrag and Hall drag, originating from long-range energy currents and spatial temperature gradients. The energy-driven effects arise in a wide temperature range, and feature an unusually strong dependence on field and carrier density. We argue that this mechanism accounts for the recently observed giant magnetodrag and Hall drag occurring at classically weak fields.

Graphene near charge neutrality (CN) hosts an intriguing electron-hole system with unique properties [1–10]. However, the lack of coupling of the neutral modes which dominate CN physics to charge modes which are easily probed in transport measurements stymies experimental progress; introducing coupling between these modes will help to advance our understanding of CN. There is a long history of employing magnetic field for such a purpose, since transport in charge-neutral plasmas is ultrasensitive to the presence of external magnetic fields [11].

A new and interesting system in which magnetotransport at CN can be probed are atomically thin graphene double layer G/hBN/G structures [12,13]. Strong Coulomb coupling between adjacent layers in these systems results in strong Coulomb drag, arising when current applied in one (active) layer induces a voltage in the adjacent (passive) layer [13–22]. Recent measurements [13] revealed drag resistance that peaks near CN and strongly depends on magnetic field, with the peak value increasing by more than an order of magnitude (and changing sign) upon application of a relatively weak *B* field. Strong magnetic field dependence of drag has been observed previously in semiconductor-based systems in the quantum Hall effect regime [23–25]. In contrast, the anomalous magnetodrag found in Ref. [13] occurs at classically weak fields $B \lesssim 1$ T.

Here we explain this puzzling behavior in terms of an energy-driven drag mechanism which involves coupled energy and charge transport [20,22] (see Fig. 1). Energy transport plays a key role because of fast vertical energy transfer due to interlayer Coulomb coupling in G/hBN/G systems [20] and relatively slow electron-lattice cooling [26,27]. As a result, current applied in one layer can create a spatial temperature gradient for electrons *in both layers*, giving rise to a thermoelectric drag voltage. The effect peaks at CN, since the thermoelectric response is large close to CN [8–10] and diminishes as $1/E_F$ upon doping away from CN [28,29]. Drag arising from this mechanism

is dominated by the thermoelectric response, which makes it largely insensitive to the electron-electron interaction strength.

Another interesting effect that can be probed in these systems is that of Hall drag. It has long been argued that, at weak coupling, no Hall voltage can arise in the passive layer in the presence of current in the active layer [30,31]. This is so because, at leading order in interaction, transferred momentum is parallel to velocity, allowing only a longitudinal "back current" to develop in the passive layer. As we shall see, a very different behavior arises at strong coupling, owing to the long-range energy currents that lead to electron-lattice temperature imbalance. Close to CN, the magnitude of the cross couplings between charge and energy currents becomes large, producing a finite Hall drag, $V_H = R_H^{\mathrm{drag}} I_{\parallel}$.

As we will see, energy currents result in Hall and magnetodrag resistances, R_H^{drag} and $R_{\parallel}^{\mathrm{drag}}$, that are large and peak near CN; see Figs. 1 and 2. These large values arise even for classically weak fields $B \sim 0.1$ T, exceeding by 2 orders of magnitude the values found in other systems [23–25] at similar fields. The mechanism based on coupled energy and charge transport predicts large and negative drag at CN that matches recent experiments [see Figs. 1(c) and 1(d)]. This mechanism also naturally leads to Hall drag because vertical energy transfer between layers does not discriminate between longitudinal and transverse heat currents since the temperature profile is a scalar field. This stands in contrast to conventional momentum driven drag, see above.

Heat current and an electric field, induced by charge current and temperature gradients, are coupled via the thermoelectric effect altered by a *B* field,

$$\mathbf{j_q} = \underline{\mathbf{Q}}\mathbf{j}, \qquad \mathbf{E} = \underline{\mathbf{Q}}\frac{\nabla T}{T}. \qquad (1)$$

Here $\underline{\mathbf{Q}}$ is a 2×2 matrix, describing the thermoelectric effect (diagonal components) and the Nernst-Ettingshausen
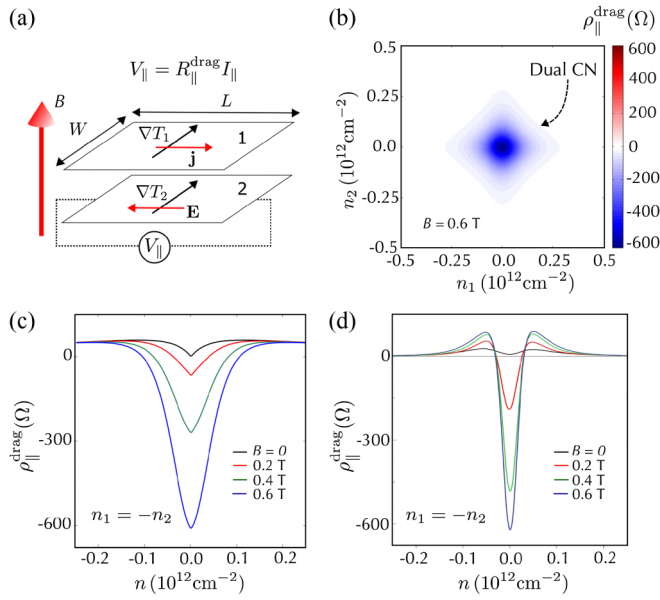
FIG. 1 (color online). Energy-driven magnetodrag in a double layer graphene heterostructure close to CN. (a) Schematic of charge current, temperature gradients, and electric field in the two layers that give rise to a *negative* $\rho_\parallel^{\mathrm{drag}}$. (b,c) Magnetodrag resistivity, $\rho_\parallel^{\mathrm{drag}}$, obtained from Eqs. (11) and (13). Parameter values: $B = 0.6$ T, $n_0 = 10^{11}$ cm^{-2}, $T = 150$ K, and $\rho_0 = (h/3e^2)$. The $B = 0$ dependence taken from the model of drag at zero B field [20,21]. (d) Experimentally measured magnetodrag resistivity in G/hBN/G heterostructures, reproduced from Ref. [13] for the same B values as in (c). Application of magnetic field leads to a giant negative drag at CN. Note the similarity of the drag density dependence, B dependence, and sign in (c) and (d).

effect (off-diagonal components). Onsager reciprocity requires that $\mathbf{Q}$ in both expressions in Eq. (1) are the same [see analysis following Eq. (9)].

We illustrate the energy-induced drag mechanism in a Hall bar geometry (Fig. 1). When a longitudinal charge current is applied in the active layer (for $B \neq 0$) a transverse (Ettingshausen) heat current develops in both layers through efficient vertical energy transfer. Nernst voltage in the passive layer results in a longitudinal magnetodrag of a *negative sign*.

To obtain the electric field in layer 2 induced by current applied in layer 1, we first need to understand the coupling of temperature profiles $T_{1,2}(\mathbf{r})$ in the two layers. Energy transport in the system can be described by

$$-\nabla_{\underline{\kappa}_1}\nabla\delta T_1 + a(\delta T_1 - \delta T_2) + \lambda\delta T_1 = -\nabla\cdot(\mathbf{Q}^{(1)}\mathbf{j}),$$
$$-\nabla_{\underline{\kappa}_2}\nabla\delta T_2 + a(\delta T_2 - \delta T_1) + \lambda\delta T_2 = 0, \quad (2)$$

with a the energy transfer rate between the two layers [20], λ the electron-lattice cooling rate, and $\delta T_i = T_i - T_0$. (Here T_0 is the lattice temperature, equal for both layers; the values λ and a will be discussed below.)

Assuming a long Hall bar, $L \gg W$, we treat the electric and heat currents as independent of the x coordinate along
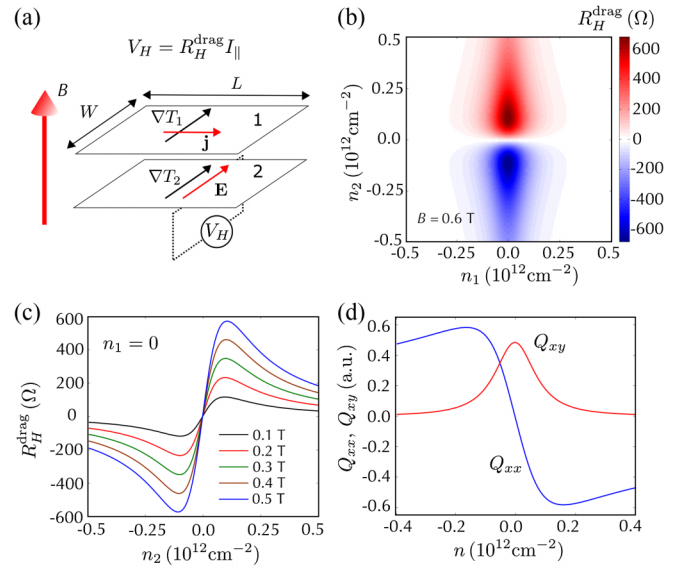
FIG. 2 (color online). (a) Schematic of charge current, temperature gradients, and electric field in the two layers of a Hall bar that produces Hall drag. (b,c) Density dependence of Hall drag resistance, predicted from Eqs. (11) and (13) for the same parameter values as in Fig. 1. (d) Density dependence of Q_{xx}, Q_{xy}, see text.

the bar (Fig. 1). In layer 1, current is injected at $x = -L/2$ and drained at $x = L/2$. In layer 2, the Hall drag voltage arising across the device, V_H, and the longitudinal drag voltage, $V_\parallel$, are evaluated as

$$V_H = \int_{-W/2}^{W/2} E_y^{(2)}dy, \qquad V_\parallel = \frac{L}{W}\int_{-W/2}^{W/2} E_x^{(2)}dy. \quad (3)$$

The electric and thermal variables may depend on the transverse coordinate y, see below.

Boundary conditions for a Hall bar require electric current to be tangential to the side boundaries, $y = \pm W/2$, and zero temperature imbalance at the ends, $x = \pm L/2$, reflecting that the current and voltage contacts act as ideal heat sinks. The electric current parallel to the boundaries $y = \pm W/2$ gives rise to the Ettingshausen heat current that may have a component transverse to the Hall bar. The divergence of this heat current, appearing on the right-hand side of Eq. (2), acts as an effective boundary delta function source in the heat transport equations. Boundary conditions can profoundly influence the symmetry of the resultant drag resistivity, see below.

We consider the case of a spatially uniform $\mathbf{Q}$ in both layers. The ideal heat sinks at $x = \pm L/2$ mean that no temperature imbalance develops in the x direction (except for some "fringing" heat currents near the contacts which give a contribution small in $W/L \ll 1$, which we will ignore in the following discussion). Since no temperature gradients are sustained in the x direction far from the ends, we can reduce our problem Eq. (2) to a quasi-1D problem with temperature profiles that only depend on the y

coordinate. As a result, the only heat source arises from the Ettingshausen effect $\underline{\mathbf{Q}}^{(1)}\mathbf{j} = (Q_{yx}^{(1)}j)\hat{\mathbf{y}}$.

To describe transport in the presence of such a source, we will expand temperature variables in both layers in a suitable orthonormal set of functions. Here it will be convenient to use eigenstates of the operator ∂_y^2 with zero Neumann boundary conditions at $y = \pm W/2$, given by

$$u_n(y) = A\cos\left(\frac{2\pi n}{W}y\right), \qquad v_n(y) = A\sin\left(\frac{2\pi(n+\frac{1}{2})}{W}y\right),$$

$A = (2/W)^{1/2}$, $n = 0, 1, 2, \ldots$ From the symmetry of the source in Eq. (2) we expect $\delta T_{1,2}(y)$ to be odd in y. Thus, only the functions $v_n(y)$ are relevant, giving

$$\delta T_{1,2}(y) = \sum_{q_n}\delta\tilde{T}_{1,2}(q_n)A\sin q_n y, \qquad q_n = \frac{2\pi(n+\frac{1}{2})}{W}.$$

For each n we obtain a pair of algebraic equations

$$\begin{aligned}
q_n^2\kappa_1\delta\tilde{T}_1 + a(\delta\tilde{T}_1 - \delta\tilde{T}_2) + \lambda\delta\tilde{T}_1 &= F_n, \\
q_n^2\kappa_2\delta\tilde{T}_2 + a(\delta\tilde{T}_2 - \delta\tilde{T}_1) + \lambda\delta\tilde{T}_2 &= 0,
\end{aligned} \qquad (4)$$

where $\kappa_{1,2} = \kappa_{xx}^{(1,2)}$ and $F_n = 2A(-1)^n Q_{yx}^{(1)}j$. Solving Eq. (4), we find the temperature profile in layer 2:

$$\delta T_2(y) = \sum_{n\geq 0}\frac{aF_n}{L_1(q_n)L_2(q_n) - a^2}v_n(y), \qquad (5)$$

where $L_i(q_n) = \kappa_i q_n^2 + a + \lambda$ ($i = 1, 2$). Since electron-lattice cooling is slow at not too high temperatures [26,27], with the corresponding cooling length values in excess of a few microns, we will suppress λ in what follows. Because the boundaries in the transverse (y direction) are free, a finite temperature imbalance between the edges can arise, given by $\Delta T = \delta T_2(y = W/2) - \delta T_2(y = -W/2)$. We find

$$\Delta T = 4A^2\sum_{n\geq 0}\frac{aQ_{yx}^{(1)}j}{L_1 L_2 - a^2} = \frac{8}{W\tilde{\kappa}}\sum_{n\geq 0}\frac{Q_{yx}^{(1)}j}{q_n^2(1 + \xi^2 q_n^2)}, \quad (6)$$

where we defined $\tilde{\kappa} = \kappa_1 + \kappa_2$ and a length scale $\xi = \sqrt{\kappa_1\kappa_2/a\tilde{\kappa}}$. We evaluate the sum using the identity

$$\sum_m \frac{1}{m^4 + c^2 m^2} = \frac{\pi^2}{2c^2}\left(1 - \frac{\tanh\pi c}{\pi c}\right)$$

($m = 1/2, 3/2, 5/2\ldots$). We obtain

$$\Delta T = \frac{WQ_{yx}^{(1)}j}{\tilde{\kappa}}G(\xi), \qquad G(\xi) = 1 - \frac{2\xi}{W}\tanh\left(\frac{W}{2\xi}\right). \quad (7)$$

Connecting ΔT with the drag voltage, and in particular determining its sign, requires taking full account of Onsager reciprocity. This analysis is presented below.

In the same way that the applied charge current, $\mathbf{j}$, in layer 1 causes a heat current (Peltier or Ettingshausen), a temperature imbalance in layer 2, ΔT, can sustain voltage

drops across the sample (thermopower or Nernst). These two effects are related by Onsager reciprocity constraints. The cross couplings in the coupled energy and charge transport equations [32] arise from

$$\begin{pmatrix} -\mathbf{j} \\ \mathbf{j_q} \end{pmatrix} = \left(\begin{array}{c|c} e\underline{\mathbf{L}}_{11}/T & e\underline{\mathbf{L}}_{12} \\ \hline \underline{\mathbf{L}}_{21}/T & \underline{\mathbf{L}}_{22} \end{array}\right)\begin{pmatrix} \nabla\mu \\ \nabla\frac{1}{T} \end{pmatrix}, \qquad (8)$$

where $\underline{\mathbf{L}}$'s are 2×2 block matrices and e is the carrier charge. In this notation, the electrical conductivity equals $\underline{\sigma} = e^2\underline{\mathbf{L}}_{11}/T$, and thermal conductivity is $\underline{\kappa} = \underline{\mathbf{L}}_{22}/T^2$. Comparing to the heat current due to an applied charge current, Eq. (1), we identify $\underline{\mathbf{L}}_{21} = -e\underline{\mathbf{Q}}\underline{\mathbf{L}}_{11}$. We will use numerical subscripts to indicate the position of the block matrices $\underline{\mathbf{L}}$ as in Eq. (8), and alphabetical superscripts to refer to the components in each block.

Onsager reciprocity demands that the cross couplings obey $\underline{\mathbf{L}}_{12}(B) = \underline{\mathbf{L}}_{21}^{\mathrm{T}}(-B)$, where B is the applied magnetic field (note the transposed matrix). In an isotropic system the off-diagonal components of $\underline{\mathbf{L}}$ obey $\underline{\mathbf{L}}^{(xy)}(B) = \underline{\mathbf{L}}^{(yx)}(-B)$. As a result, Onsager reciprocity reduces to

$$\underline{\mathbf{L}}_{12}(B) = \underline{\mathbf{L}}_{21}(B) \qquad (9)$$

in an isotropic system. Applying Eq. (9) to Eq. (8) in an open circuit, we find $\mathbf{E} = -e^{-1}\nabla\mu = T^{-1}\underline{\mathbf{L}}_{11}^{-1}\underline{\mathbf{Q}}\underline{\mathbf{L}}_{11}\nabla T$. For an isotropic system $\underline{\mathbf{Q}} = Q_{xx}\mathbf{1} + iQ_{xy}\sigma_2$, $\underline{\mathbf{L}} = L_{xx}\mathbf{1} + iL_{xy}\sigma_2$, so that $[\underline{\mathbf{Q}}, \underline{\mathbf{L}}] = 0$, which gives Eq. (1).

Several different regimes arise depending on the relation between the interlayer cooling length ξ and the bar width W. Using Eqs. (3) and (1) we obtain

$$\begin{pmatrix} V_\parallel \\ V_H \end{pmatrix} = \begin{pmatrix} R_\parallel^{\mathrm{drag}} & -R_H^{\mathrm{drag}} \\ R_H^{\mathrm{drag}} & R_\parallel^{\mathrm{drag}} \end{pmatrix}\begin{pmatrix} I_\parallel \\ 0 \end{pmatrix}, \qquad (10)$$

giving the magnetodrag and Hall drag resistance values

$$R_H^{\mathrm{drag}} = \frac{-G(\xi)}{T\tilde{\kappa}}Q_{xy}^{(1)}Q_{xx}^{(2)}, \qquad R_\parallel^{\mathrm{drag}} = \frac{-LG(\xi)}{WT\tilde{\kappa}}Q_{xy}^{(1)}Q_{xy}^{(2)}, \qquad (11)$$

where we used $Q_{xx} = Q_{yy}$ and $Q_{xy} = -Q_{yx}$ for an isotropic system. For slow interlayer cooling, $\xi \gg W$, we have $G \to 0$, giving vanishingly small $R_{H,\parallel}^{\mathrm{drag}}$. For fast interlayer cooling, $\xi \ll W$, we have $G \to 1$. In this case $R_{H,\parallel}^{\mathrm{drag}}$ saturates to a universal value independent of the interlayer cooling rate. For typical device parameters, we estimate $\xi \approx 40$ nm at $T = 300$ K [20]. Since L, W are a few microns for typical graphene devices, we expect them to be firmly in the $G = 1$ regime, with the Hall drag and magnetodrag attaining universal values independent of the electron-electron interaction strength.

To describe the density and B-field dependence, we use a simple model for $\underline{\mathbf{Q}}$. Measurements indicate [8,9] that

thermopower and the Nernst effect in graphene are well described by the Mott formula [33], giving

$$\underline{\mathbf{Q}} = \frac{\pi^2}{3e} k_B^2 T^2 \underline{\rho} \frac{\partial[\underline{\rho}^{-1}]}{\partial \mu}, \qquad \underline{\rho} = \begin{pmatrix} \rho_\parallel & \rho_H \\ -\rho_H & \rho_\parallel \end{pmatrix}, \quad (12)$$

with ρ the resistivity, $e < 0$ the electron charge, and μ the chemical potential. We use a simple phenomenological model [34] relevant for classically weak B fields

$$\rho_\parallel = \frac{\rho_0}{\sqrt{1 + n^2/n_0^2}}, \qquad \rho_H = \frac{-Bn}{e(n^2 + n_0^2)}, \qquad (13)$$

where ρ_0 is the resistivity peak value at the Dirac point, n is the carrier density, and parameter n_0 accounts for broadening of the Dirac point due to disorder. We account for disorder broadening of the density of states, $dn/d\mu = (n^2 + n_0^2)^{1/4}[2/(\pi\hbar^2 v_F^2)]^{1/2}$.

From Eqs. (11)–(13) and the Wiedemann-Franz relation for κ, we obtain $\rho_\parallel^{\text{drag}} = (W/L)R_\parallel^{\text{drag}}$ and R_H^{drag}. The modeling results are shown in Figs. 1(b), 1(c), 2(b), and 2(c), where we used the parameter values $n_0 = 10^{11}$ cm^{-2}, $\rho_0 = (h/3e^2)$, and a representative temperature, $T = 150$ K. These values match device characteristics (disorder broadening, n_0, and peak resistivity, ρ_0) described in Ref. [13]. As a sanity check, we plot the components of $\mathbf{Q}$ [in Fig. 2(d)] which show the behavior near CN matching thermopower and Nernst effects measured in graphene [8,9].

Analyzing magnetodrag, we find that $\rho_\parallel^{\text{drag}}$ peaks at dual CN, $n_1 = n_2 = 0$, taking on large and *negative* values [Figs. 1(b) and 1(c)]. The magnetodrag peak exhibits a steep B dependence, $\rho_{\parallel,\text{peak}}^{\text{drag}} \propto -B^2$, bearing a striking resemblance to measurements reproduced in Fig. 1(d). In particular, our model explains the negative sign of the measured magnetodrag.

Hall drag is large and sign changing [see Figs. 2(b) and 2(c)], taking on values consistent with measurements [35]. Interestingly, the map in Fig. 2(b) indicates that the sign of R_H^{drag} is controlled solely by carrier density in layer 2, breaking the $n_1 \leftrightarrow n_2$ symmetry between layers. This behavior does not contradict Onsager reciprocity. It arises as a consequence of the asymmetric boundary conditions for the Hall bar: free boundary at $y = \pm W/2$ and ideal heat sinks at the ends, $\delta T(x = \pm L/2) = 0$. This allows for finite temperature gradients to be sustained across the bar but not along the bar; see Fig. 2(a).

For other geometries, the temperature gradient can be obtained by balancing the heat flux due to thermal conductivity against the net heat flux in the two layers, $(\kappa_1 + \kappa_2)\nabla\delta T = \underline{\mathbf{D}}\underline{\mathbf{Q}}^{(1)}\mathbf{j}_1$ [see Eq. (24) of Ref. [22]]. The quantity $\underline{\mathbf{D}}$ can in principle be obtained by solving heat transport equations. Adopting the same approach as above, we find a magneto and Hall-drag resistivity

$$\underline{\rho}^{\text{drag}} = \frac{1}{T\tilde{\kappa}}\underline{\mathbf{Q}}^{(2)}\underline{\mathbf{D}}\underline{\mathbf{Q}}^{(1)}, \qquad \mathbf{E}_2 = \underline{\rho}^{\text{drag}}\mathbf{j}_1. \quad (14)$$

For isotropic heat flow, $\underline{\mathbf{D}} = \mathbf{1}$. In this case, since $\underline{\mathbf{Q}}^{(1)}$ and $\underline{\mathbf{Q}}^{(2)}$ commute, the resulting drag is layer symmetric, $n_1 \leftrightarrow n_2$ [22]. In particular, Hall drag for $\underline{\mathbf{D}} = \mathbf{1}$ vanishes on the diagonal $n_1 = -n_2$. In contrast, for anisotropic heat flow, such as that discussed above, we expect a generic tensor $\underline{\mathbf{D}} \neq \mathbf{1}$ and thus no layer symmetry.

We wish to clarify, in connection to recent measurements, [35] that layer symmetry $n_1 \leftrightarrow n_2$ implies a swap of current and voltage contacts. Layer symmetry, corresponding to $\underline{\mathbf{D}} = \mathbf{1}$ in Eq. (14), will therefore only hold for Hall bars equipped with wide voltage contacts, for which the contact and the bar widths are comparable. This is indeed the case for the cross-shaped devices used in Ref. [13]. However, it is not the case for a Hall bar with *noninvasive* voltage probes which are much narrower than the bar width, as assumed in our analysis above. Noninvasive probes, which have little effect on temperature distribution in the electron system, translate into $\underline{\mathbf{D}} \neq \mathbf{1}$ and no layer symmetry.

In summary, magnetic field has a dramatic effect on drag at CN because it induces strong coupling between neutral and charge modes, which are completely decoupled in the absence of a magnetic field for a uniform system. Field-induced mode coupling leads to a giant drag that dwarfs the conventional momentum drag contribution as well as a remnant drag due to spatial inhomogeneity [20]. Our estimates indicate that these two contributions are orders of magnitude smaller than the predicted magnetodrag, which also has an opposite sign. The giant magnetodrag and Hall drag values attained at classically weak magnetic fields, along with the unique density dependence and sign, make these effects easy to identify in experiment. The predicted magnetodrag is in good agreement with findings in Ref. [13]. Magnetic field, coupled with drag measurements at CN, provides a unique tool for probing the neutral modes in graphene.

[1] J. Gonzales, F. Guinea, and M. A. H. Vozmediano, Nucl. Phys. **B424**, 595 (1994); Phys. Rev. B **59**, R2474 (1999).
[2] D. E. Sheehy and J. Schmalian, Phys. Rev. Lett. **99**, 226803 (2007).
[3] D. T. Son, Phys. Rev. B **75**, 235423 (2007).
[4] O. Vafek, Phys. Rev. Lett. **98**, 216401 (2007).
[5] A. B. Kashuba, Phys. Rev. B **78**, 085415 (2008).
[6] L. Fritz, J. Schmalian, M. Müller, and S. Sachdev, Phys. Rev. B **78**, 085416 (2008).
[7] M. Müller, L. Fritz, and S. Sachdev, Phys. Rev. B **78**, 115406 (2008).

[8] Y. M. Zuev, W. Chang, and P. Kim, Phys. Rev. Lett. **102**, 096807 (2009).

[9] P. Wei, W. Bao, Y. Pu, C. N. Lau, and J. Shi, Phys. Rev. Lett. **102**, 166808 (2009).

[10] J. G. Checkelsky and N. P. Ong, Phys. Rev. B **80**, 081413(R) (2009).

[11] L. P. Pitaevskii, E. M. Lifshitz, *Physical Kinetics* (Pergamon, Oxford, 1981).

[12] L. Britnell *et al.*, Science **335**, 947 (2012).

[13] R. V. Gorbachev *et al.*, Nat. Phys. **8**, 896 (2012).

[14] S. Kim, I. Jo, J. Nah, Z. Yao, S. K. Banerjee, and E. Tutuc, Phys. Rev. B **83**, 161401 (2011).

[15] W.-K. Tse and S. D. Sarma, Phys. Rev. B **75**, 045333 (2007).

[16] B. N. Narozhny, Phys. Rev. B **76**, 153409 (2007).

[17] E. H. Hwang, R. Sensarma, and S. D. Sarma, Phys. Rev. B **84**, 245441 (2011).

[18] N. M. R. Peres, J. M. B. Lopes dos Santos, and A. H. C. Neto, Europhys. Lett. **95**, 18 001 (2011).

[19] M. I. Katsnelson, Phys. Rev. B **84**, 041407 (2011).

[20] J. C. W. Song and L. S. Levitov, Phys. Rev. Lett. **109**, 236602 (2012).

[21] B. N. Narozhny, M. Titov, I. V. Gornyi, and P. M. Ostrovsky, Phys. Rev. B **85**, 195421 (2012).

[22] J. C. W. Song, D. A. Abanin, and L. S. Levitov, Nano Lett. **13**, 3631 (2013).

[23] N. K. Patel, E. H. Linfield, K. M. Brown, M. Pepper, D. A. Ritchie, and G. A. C. Jones, Semicond. Sci. Technol. **12**, 309 (1997).

[24] H. Rubel, A. Fischer, W. Dietsche, K. von Klitzing, and K. Eberl, Phys. Rev. Lett. **78**, 1763 (1997).

[25] M. P. Lilly, J. P. Eisenstein, L. N. Pfeiffer, and K. W. West, Phys. Rev. Lett. **80**, 1714 (1998).

[26] M. W. Graham, S.-F. Shi, D. C. Ralph, J. W. Park, and P. L. McEuen, Nat. Phys., **9**, 103 (2012).

[27] A. C. Betz, S. H. Jhang, E. Pallecchi, R. Ferreira, G. Féve, J.-M. Berroir, and B. Placais, Nat. Phys., **9**, 109 (2012).

[28] J. M. Ziman, *Principles of the Theory of Solids* (Cambridge University Press, Cambridge, England, 1979).

[29] E. H. Hwang, E. Rossi, and S. D. Sarma, Phys. Rev. B **80**, 235415 (2009).

[30] A. Kamenev and Y. Oreg, Phys. Rev. B **52**, 7516 (1995).

[31] M. C. Bonsager, K. Flensberg, B. Y.-K. Hu, and A.-P. Jauho, Phys. Rev. Lett. **77**, 1366 (1996). The authors note that Hall drag vanished for systems with inversion symmetry and when the carriers in the active layer can be described by a drifted Fermi-Dirac distribution.

[32] H. B. Callen, Phys. Rev. **73**, 1349 (1948).

[33] M. Jonson and S. M. Girvin, Phys. Rev. B **29**, 1939 (1984).

[34] D. A. Abanin *et al.*, Science **332**, 328 (2011) and accompanying online supplement.

[35] A. K. Geim, private communication